







Synthesis of Biogenic Gold Nanoparticles by Using Sericin Protein from *Bombyx mori* Silk Cocoon and Investigation of Its Wound Healing, Antioxidant, and Antibacterial Potentials

Gitishree Das ¹, Sujin Seo ², In-Jun Yang ³, Ly Thi Huong Nguyen ³, Han-Seung Shin ², Jayanta Kumar Patra ¹

¹Research Institute of Integrative Life Sciences, Dongguk University-Seoul, Goyangsi, Republic of Korea; ²Department of Food Science & Biotechnology, Dongguk University-Seoul, Goyangsi, Republic of Korea; ³Department of Physiology, College of Korean Medicine, Dongguk University, Gyeongju, Republic of Korea

Correspondence: Jayanta Kumar Patra, Research Institute of Integrative Life Sciences, Dongguk University-Seoul, Goyangsi, 10326, Republic of Korea, Tel +82-31-961-5625, Email jkpatra@dongguk.edu

Introduction: A number of biological wastes and factory waste materials have been tested recently for the eco-friendly biosynthesis of nanoparticles. Sericin protein (SSP) is usually removed from the silk cocoon during the degumming process in the process of making the silk, and this sericin protein is normally thrown away by the sericulture industries as waste materials. It is found that this sericin protein possesses a number of biological properties.

Methods: Considering this, in the present study, an effort has been made to biosynthesize gold nanoparticles (SSP-AuNPs) using the waste sericin solution as the reducing and capping agent and investigate its biopotential in terms of its wound healing, antioxidant and antibacterial activities.

Results: The synthesis of SSP-AuNPs was perceived by the visual color change and confirmed by UV-Vis spectroscopy with absorption maxima at 522 nm. Further characterization of SSP-AuNPs was done by TEM, EDS, XRD, FTIR, DLS, zeta potential, TGA, AFM, etc. The size of SSP-AuNPs was found out to be 54.82 nm as per the particle size analyzer and the zeta potential is -19.8 mV. The SSP-AuNPs displayed promising wound healing potential of 70.96 and 69.76% wound closure rate at 5 and 10 $\mu\text{g/mL}$ respectively as compared to 74.91% by the *Centella asiatica* taken as a positive control. It also exhibited promising antioxidant potential in terms of the DPPH, ABTS free radical scavenging, reducing power potential, and total antioxidant capacity. Besides, the SSP-AuNPs also displayed significant antibacterial activities against the tested pathogenic bacterial with the diameter of inhibition zones ranging between 12.10 and 14.96 mm as compared to the positive control cephalexin that displayed inhibition zones ranging between 12.08 and 13.24 mm.

Discussion: Taken together, SSP-AuNPs could serve as an interesting candidate for food, cosmetics, and biomedical fields in the applications of wound healing, cosmetics, antibacterial bandages, and ointments, etc.

Keywords: silk cocoon, biowaste, sericin, silk protein, biosynthesis, wound healing, antioxidant, antibacterial, gold nanoparticles, wound healing

Introduction

Nanotechnology research is a multidisciplinary field interposing the science of biotechnology and materials engineering together, and many significant advancements have been achieved in this interdisciplinary research that benefited humankind.¹ Currently, there have been many applications of colloidal nanoparticles in biomedical fields such as imaging, catalytic, drug delivery, antimicrobial agents, etc.^{2,3} Further, the physicochemical properties of the colloidal nanoparticles including the optical, electronic, magnetic, and luminescent properties greatly influence the shape, size, and composition of these

nanoparticles thereby influencing their overall performances.^{1,2,4,5} As per the requirement, the synthesis of the nanoparticles has been done by several specific methods and principles.³ The bio-based nanoparticle synthesis methods are getting a higher interest rate than other synthesis methods since the synthesis of nanoparticles using the conventional physical and chemical method is a very tedious process, it is more expensive, and used hazardous chemicals.^{1,3,6} These biological methods of nanoparticles using plant parts, extracts, microorganisms, fungi, etc, are cheaper, eco-friendly, and could play a significant role in the applications of the synthesized nanoparticles in the biomedical fields.^{1,7} Gold nanoparticles have distinctive physicochemical characteristics that vary from conventional gold metals and these characteristics are specifically adjustable by regulating the shape and size of the gold nanoparticles.^{3,8,9} Mostly like other metal nanoparticles, the gold nanoparticle biosynthesis by the use of green methods using a natural polymer as the reducing and capping agent has attracted massive attention in recent years, as it is technologically important in various fields like tissue engineering, electronic, biosensing, anti-bacterial, drug delivery and cancer therapy, etc.^{3,7,8,10–12}

The cocoons of *Bombyx mori* are natural silk compounds having multifunctional properties with exclusive structure. The *B. mori* cocoons are the main source of silk products and are composed of an inner shell (fibroin, 70%) and a covered outer shell (sericin, 30%).¹³ Sericin is a natural glycoprotein polymer produced by silkworms.¹⁴ It is removed in large amounts as a biowaste material during the processing of silk cocoons for the production of silk by the textile industries.^{15,16} It is estimated that, globally, around 50 thousand tons of sericin produced from 4 lakh tons of dry cocoons, are generally discarded in wastewater by the textile industries.¹⁷ This waste sericin produces high chemical wastes and thus contaminates the water.^{18,19} However, sericin contains hydroxyl groups, carboxyl groups, and amino groups.^{15,20–22} Sericin is having substantial biologically active properties that permit its application in numerous fields. It possesses various biological activities such as antitumor activities, immunomodulatory, suppression of elastase, UV-resistant and moisture absorbing properties, antioxidation, kinase activity, and tyrosinase activity; it also promotes cell growth, wound healing, anticancer and anticoagulant properties.^{13,16,23–26} Owing to their biodegradation, biocompatibility, and strong ability to stimulate cell differentiation, it is appropriate for bone filling applications and it has the prospect to provide therapeutic medicine. As it supports cell viability, the sericin compounds have potential in bone-associated applications and tumor therapy as drug delivery systems.^{27,28}

In the current research, after considering the biological potential of sericin in various applications, an attempt has been made to extract the raw sericin from the silk cocoons of *Bombyx mori* and synthesize the gold nanoparticles using the sericin extract solution as the bio-reducing agent and investigate its bio-potentials in terms of its antioxidant, antibacterial and wound healing activities.

Materials and Methods

Collection, Extraction, and Purification of Sample

Raw silk cocoons of *Bombyx mori* were purchased from a local sericulture farm in Gyeonggi-do province of the Republic of Korea and immediately transferred to the laboratory in polythene bags. The outer surface wastes were removed from the silk cocoon by thoroughly cleaning them in running water and were surface-dried over the tissue paper. Further, the silk cocoon was cut into small pieces of 10 mm × 10 mm size. The extraction of sericin from the silk cocoon was carried out by previously established procedure.²⁹ Briefly, around 50 gm of silk cocoon was taken in a conical flask and to which 200 mL of an alkali solution (0.2% of sodium carbonate) was added and it was boiled at 121 °C for 1 hr. The extracted sericin solution (SSP) was filtered by using Whatman No. 1 filter paper and then it was concentrated to one-third of its volume at 60 °C and further, it was dialyzed against the distilled water at room temperature for 72–96 h. The concentration of the purified sericin solution was calculated by Lowry's method. Further, the dialyzed sericin solution was freeze-dried and stored in airtight vials.

Synthesis of Gold Nanoparticles Using Sericin Solution (SSP)

The synthesis of sericin-mediated gold nanoparticles was carried out using the standard procedure as described by Akturk et al.³⁰ Before the synthesis, different dilutions (100%, 50%, 25%, 12.5%, 6.25%, 3.125%, 1.56%, and 0.78%) of the purified sericin solution were made, briefly, 10 mL of the gold (III) chloride solution (1.0 mM, H₂AuCl₄·3H₂O) was taken in different

50-mL Erlenmeyer flasks and to them, 10 mL of different dilutions of sericin solution was added separately dropwise for around 10 min followed by exposure to the UV radiation by the UV lamps in a clean bench for about 24 h at room temperature. The visual change in the color of the reaction mixture from light yellow to purple-red-violet color confirms the synthesis of gold nanoparticles. After 24 h, the reaction mixture was centrifuged at 11,000 rpm for 25 min in a high-speed ultra centrifuge machine followed by repeated washing using the double-distilled water. Further, the supernatant was discarded and the pellet (biosynthesized SSP-AuNPs) was collected, dried, and kept in an airtight container for further analysis.

Characterization of Biosynthesized SSP-AuNPs

The bio-based SSP-AuNPs were characterized using different analytical methods like UV-VIS spectroscopy, transmission electron microscopy (TEM), energy-dispersive X-ray (EDS), zeta potential and particle size analysis, X-ray powder diffraction analysis (XRD), Fourier transform infrared spectroscopy (FTIR), thermogravimetric analysis (TGA), and atomic force microscopy (AFM) analysis by following the standard established procedures as mentioned in previously published articles.^{31–33}

UV-Vis Spectral Analysis of the Biosynthesized SSP-AuNPs

The UV-Vis spectra of the biosynthesized SSP-AuNPs were checked by measuring the absorbance spectra of the reaction mixture using a UV-Vis spectrophotometer (Multiskan Go; Thermo Scientific, Waltham, USA) from 300 to 700 nm for 1 day. The change in the color of the reaction mixture was also recorded.

The TEM and EDS Analysis of SSP-AuNPs

The size and surface morphology of the biosynthesized SSP-AuNPs were analyzed by transmission electron microscopy (TEM, Tecnai G2 F20/FEI) and the elemental compositions of the SSP-AuNPs were analyzed by the EDS machine attached to the TEM. For, the TEM analysis, the samples were prepared by diluting and sonicating the SSP-AuNPs solutions into different dilutions, and then the copper grids were put on the solution. Then, the copper grid was removed from the solution and air dried and then analyzed in the TEM machine.

The Size and Zeta Potential Study of Biosynthesized SSP-AuNPs

The size distribution through DLS (Dynamic Light Scattering) and the zeta potential of the biosynthesized SSP-AuNPs were evaluated by the zeta potential machine (Malvern Zetasizer Nano-ZS machine, Malvern, UK) at the temperature of 25°C.

The XRD Analysis of SSP-AuNPs

The crystal structure of the biosynthesized SSP-AuNPs was determined by the XRD machine using the Cu-K α radiation at 40 mA and 30 kV at an angle of 2θ (X'pert MRD; Panalytical Almelo, The Netherlands).

FTIR Analysis of the Biosynthesized SSP-AuNPs

The FT-IR spectra of the sericin extract and the biosynthesized SSP-AuNPs were determined by using the FT-IR spectrophotometer (Nicolet iS5 FTIR Spectrometer, ThermoFisher Scientific) within a range of 400–4000 cm^{-1} in transmittance mode. About, 2 μL of the sericin solution/SSP-AuNPs was poured on the sample collection point and was analyzed using the inbuilt computer software attached to the machine. Using different modes of vibration the occurrence of diverse types of functional groups in the sample was detected.

The TGA/DTG (Thermo-Gravimetric and Derivative Thermogravimetric Analysis) of the Biosynthesized SSP-AuNPs

The thermal stability and composition of the biosynthesized SSP-AuNPs were determined by a TGA machine (pyris TGA/N-1000, SNACK, USA). For TGA/DTG analysis, around 100 mg of the powdered SSP-AuNPs sample was placed in an alumina pan and heated from 25°C to 900°C at a ramping time of 10°C/minute.

The AFM (Atomic Force Microscopy) Analysis of the Biosynthesized SSP-AuNPs

The surface nature and morphology of the biosynthesized SSP-AuNPs were carried out by using an atomic force microscope (NanoMan/Multimode8 AFM machine, Veeco/Bruker Nano Surfaces, USA). The SSP-AuNPs samples were diluted and dropped on a Si wafer slide and dried at room temperature before measurement.

Evaluation of the Biological Potential of the Biosynthesized SSP-AuNPs

The biological potential of the biosynthesized SSP-AuNPs was investigated by the wound healing, antioxidant, and antibacterial assays using the standard established protocols.

The Wound Healing Potential of the SSP-AuNPs

The Cell Viability (Toxicity) Assay of SSP-AuNPs

For cell viability assay of the obtained SSP-AuNPs, the HaCaT cells were cultured in EMEM (Lonza, Walkersville, MD, USA) at a low concentration of Ca^{2+} (0.03 mM), supplemented with 10% FBS and 1% penicillin/streptomycin (Invitrogen Inc., Carlsbad, CA, USA), at 37°C in a humidified incubator. The effects of SSP-AuNPs on the viability of HaCaT cells were examined using MTT assays.³⁴ HaCaT cells were seeded at a density of 5×10^4 cells/well to 96-well plates. After 24 h, cells were treated with SSP-AuNPs (5, 10, 25 $\mu\text{g/mL}$) for 24 h. After treatment, the culture medium was removed, then 100 μL fresh medium and 10 μL of MTT reagent (5 mg/mL) (Sigma-Aldrich, St. Louis, MO, USA) were added to each well. The plate was incubated at 37°C for 4 h. The medium was removed and 50 μL DMSO was added to each well and incubated for 30 min. Absorbance was measured at 570 nm using a microplate reader (Tecan, Mannedorf, Switzerland).

Scratch Wound Assay of SSP-AuNPs

For scratch wound assay of SSP-AuNPs, the HaCaT cells were seeded at a density of 4×10^5 cells/well on 12-well plates and allowed to achieve 100% confluence.^{34,35} Then, the cells were scratched and treated with SSP-AuNPs samples (5, 10, 25 $\mu\text{g/mL}$) or *Centella asiatica* extract (positive control, 100 $\mu\text{g/mL}$; United States Pharmacopeia (USP) Reference Standard, purchased from Sigma Aldrich). The images of scratch gap width for each time-point were captured by Lionheart FX Automated imaging system and measured using Gen5 Imager software (Biotek Instruments Inc., Winooski, VT, USA). The rate of wound closure rate was calculated using the following formula: wound closure Rate = (original scratch gap width - open gap width on 24h)/original scratch gap width *100.

The Antioxidant Potential of SSP-AuNPs

The antioxidant potential of the SSP-AuNPs was determined by four different antioxidant assays such as the 1,1-diphenyl-2-picrylhydrazyl (DPPH) free-radical scavenging, 2,2-azino bis(3-ethylbenzothiazoline-6-sulfonic acid) (ABTS) free-radical scavenging, reducing power assays and the total antioxidant capacity (TAC) following the standard protocol as described by Patra and Baek³³ The effective concentration that exhibited 50 % of scavenging was also calculated in terms of the IC_{50} or the $\text{IC}_{0.5}$ values.

DPPH Free Radical Scavenging Assay

The DPPH free radical scavenging of the biosynthesized SSP-AuNPs was determined by the standard protocol as described by Patra et al.³⁶ Briefly, three different concentrations (25, 50, and 100 $\mu\text{g/mL}$) of the SSP-AuNPs and BHT (butylated hydroxytoluene) taken as the standard reference compound were taken for the assay. The absorbance of the reaction mixtures was measured at 517 nm using the microplate reader (Multiskan Go; Thermo Scientific, Waltham, MA, USA) and the results were calculated as per the following equation:

$$\text{Percentage scavenging} = \frac{C_{\text{abs}} - T_{\text{abs}}}{C_{\text{abs}}} \times 100 \quad (1)$$

where C_{abs} is the absorbance of the control sample and T_{abs} is the absorbance of the treatment sample.

ABTS Free Radical Scavenging Assay

The ABTS radical scavenging activity of SSP-AuNPs was determined as per the standard procedure of Das et al.³⁷ Before the experiment, stock solutions of 7.4 mM ABTS and 2.6 mM of potassium persulfate were prepared and mixed equally and kept in dark for 12 h. For the experiment, briefly, 30 μL of different concentrations of the SSP-AuNPs (25, 50, and 100 $\mu\text{g/mL}$) and the standard BHT were added to the vials containing 270 μL of the ABTS mixture solution and

kept in dark for 2 h. After incubation, the absorbance of the mixture solution was measured at 734 nm, and the scavenging percentage of ABTS free radical was calculated by following equation 1.

Reducing Power Assay

The reducing power of the biosynthesized SSP-AuNPs was determined by the standard procedure as described by Patra et al.³⁸

Briefly, 50 μL each of SSP-AuNPs/BHT (25, 50, and 100 $\mu\text{g}/\text{mL}$), phosphate buffer (0.2 M, pH 6.6), and potassium ferricyanide (1%) are mixed and incubated at 50 $^{\circ}\text{C}$ for 20 min in dark. After incubation, the reaction was terminated by adding 50 μL of TCA (10%) followed by centrifugation at 3000 rpm for 10 min. Then, 50 μL of the supernatant was collected, and to it, distilled water was added to make up the volume to 100 μL then, 10 μL of FeCl_3 (0.1%) was added and the mixture was kept for 10 min at room temperature. Lastly, the absorbance of the reaction mixture was measured at 700 nm and the results were presented in terms of the absorbance value.

Total Antioxidant Capacity

The TAC of the SSP-AuNPs was determined using the assay kit (MAK334, Sigma-Aldrich) by the standard protocol of the manufacturer. The absorbance was measured at 570 nm. The TAC values of the sample were calculated according to the following equation:

$$\text{TAC } (\mu\text{M Trolox equivalents}) = \frac{T_{\text{abs}} - C_{\text{abs}}}{\text{Slope } (\mu\text{M}^{-1})} \times n$$

where C_{abs} is the absorbance of the control sample, T_{abs} is the absorbance of the treatment sample and n is the sample dilution number. The slope is calculated from the linear calibration formula generated from the standard curve.

The Antibacterial Potential of SSP-AuNPs

The antibacterial effect of the biosynthesized SSP-AuNPs was determined against four different foodborne pathogenic bacteria (*Escherichia coli* O157: H7 ATCC 23514, *Enterococcus faecium* DB01, *Salmonella enterica* KCCM 11806 and *Salmonella* Typhimurium KCTC 1925) using a standard disc diffusion assay as described by Patra and Baek.³³ Prior to use, the pathogenic bacteria were subcultured in the nutrient broth media. For the disc diffusion assay, a paper disc of 100 μg of SSP-AuNPs/disc and 10 μg of cephalexin/disc (standard antibiotic) was prepared. The pathogens were spread uniformly on the agar plates and the filter paper discs were placed over them and incubated for 24 h at 37 $^{\circ}\text{C}$. The antibacterial activity of the SSP-AuNPs and standard cephalexin was calculated by measuring the diameter of the zone of inhibition after the incubation period.

Further, to determine the minimum inhibitory concentration (MIC) of the SSP-AuNPs, the twofold serial dilutions procedure was followed.³⁹ Before the test, different concentrations of the AuNPs were prepared by twofold serial dilution method, and to them, about 10 μL of different pathogenic bacterial culture was added separately and incubated at 37 $^{\circ}\text{C}$ for overnight. After the incubation period, the MIC value was calculated by visual observation. The lowest concentration of the sample that did not show any distinctly visible growth of the bacteria in the solution is measured as the MIC of the SSP-AuNPs. Whereas the corresponding concentration of the SSP-AuNPs that showed no growth of the bacteria on the agar plate was measured as the minimum bactericidal concentration (MBC).

Statistical Analysis of the Biosynthesized SSP-AuNPs

All experiments were performed in triplicates and the results are presented as the mean value and standard deviations. Further, the statistical analysis data of SSP-AuNPs was performed by ANOVA (one-way analysis of variance) followed by Duncan's multiple range test at a 5% level of significance ($P < 0.05$) using SPSS version 27.0 (IBM Corp., Armonk, NY, USA). Linear regression analysis and Pearson's correlation analysis were also conducted using the SPSS software to estimate the association between the parameters.

Results and Discussion

The Biosynthesis and Characterization of SSP-AuNPs

Sericin which is hydrophilic has 18 amino acids and most of which have the amino, carboxyl, and hydroxyl groups.⁴⁰ It has been reported that the synthesis of gold nanoparticles from the precursor compound was possible due to the action of the phenylalanine, tryptophan, and tyrosine present in sericin which is involved in the redox reaction.^{40,41} In the current study, sericin was extracted from the silk cocoon by the degumming process. After extraction followed by purification using dialysis, the concentration of the purified sericin was found to be 3.59% as calculated by Lowry's method by taking bovine serum albumin as the standard ($R^2 > 0.99$). The biosynthesis of the SSP-AuNPs was carried out by taking the sericin biowaste solution (Figure 1A), a protein polymer from the silk cocoon as the reducing and capping agent. In the current investigation, different dilutions of sericin solution (100%, 50%, 25%, 12.5%, 6.25%, 3.125%, 1.56% and 0.78%) was used for the biosynthesis of gold nanoparticles and it was concluded that the synthesis of NPs was not possible at the higher concentration of SSP extracts (100%, 50%, 25%, 12.5%) as well at very low SSP extract concentration (0.78%) as evident from no visual color change in the reaction mixture. However, there was visible color changes in the three reaction mixture solutions containing 6.25%, 3.13%, and 1.56% SSP extract, and the best result was obtained at the concentration of 1.56% with distinct purple-red-violet coloration and a clear UV-Vis spectral peak of the reaction solution (Figure 1B and C). Hence, we have used the SSP-AuNPs that were synthesized with a sericin concentration of 1.56% for further characterization and application studies. Sericin has been reported to possess a number of bioactive potentials, which is an important cause for selecting it to use it as a reducing agent in the synthesis process.

After its synthesis, the biosynthesized SSP-AuNPs were characterized by various standard methods such as UV-Vis-spectral analysis, TEM, EDS, zeta potential and dynamic light scattering-particle size analysis, XRD, FT-IR, TGA, and AFM analysis, etc. During the process of nanoparticle synthesis, the visual color change confirmed the conversion of gold ions to the gold nanoparticle (Figure 1B). The gradual change of color from transparent to purple-red-violet color (Figure 1B) confirmed the biosynthesis of SSP-AuNPs, and further, it was also evidenced by the UV-Vis spectral analysis results (Figure 1C). The surface plasmon resonance value was observed at 522 nm wavelength at 24 h (Figure 1C), which is specific for gold nanoparticles as evident from previously reported results.^{30,40,42,43} This surface plasmon resonance was detected due to the movement of free electrons in the conduction band because of the interaction with the electromagnetic radiation.^{40,44}

Commonly, TEM is considered as a great tool to gather data about the size, dispersion, and morphology of the synthesized nanoparticles.⁴⁵ The TEM analysis results revealed that the biosynthesized SSP-AuNPs are nearly spherical and are well dispersed in shape (Figure 2A), with no noticeable accumulation.⁴⁶ The selected area electron diffraction (SAED) pattern provided further evidence of the crystalline nature of the SSP-AuNPs (Figure 2B). The average size of the obtained nanoparticle in the TEM image was calculated as 10.819 nm by the ImageJ software (Figure 2C). The TEM image was taken after 2 months of the biosynthesis after completing all reactions, and the particles did not agglomerate which confirmed that the samples are stable (Figure 2A). The elemental composition of the SSP-AuNPs was detected by EDS analysis and the results, showed that the SSP-AuNPs are mainly composed of Au (98.11%) along with very negligible other signal peaks like Si, Cu, and O (1.88%) (Figure 2D).

The size distributions (hydrodynamic diameter) and surface charges of the SSP-AuNPs were estimated through the DLS and zeta potential study. The Z-average hydrodynamic diameter (size distribution) of SSP-AuNPs is calculated as 54.82 nm with a 0.307 PDI (polydispersity index) value (Figure 3A) and the zeta potential was found out -19.80 mV (Figure 3B). It is seen that the size distribution from the TEM image and size distribution by the DLS instrument is different and the reason behind this difference is that the TEM analysis is a number-based technique and it only gives emphasis to the smallest components in the exposed surface of the image whereas the DLS analysis is an intensity-based technique and puts higher emphasis on the large particle sizes in the mixture solution, with the solvent layer and thus sometimes they get aggregated. Besides, the DLS measures the hydration sphere diameter of the nanoparticles and it is a cumulative analysis method it measures hundreds and thousands of nanoparticles in the mixture solution; hence, its value is higher than that of the TEM size. This discussion on the particle size distribution has been debated in previously published literature.⁴⁷ The high negative charge zeta potential of the SSP-AuNPs represents the long period stability of

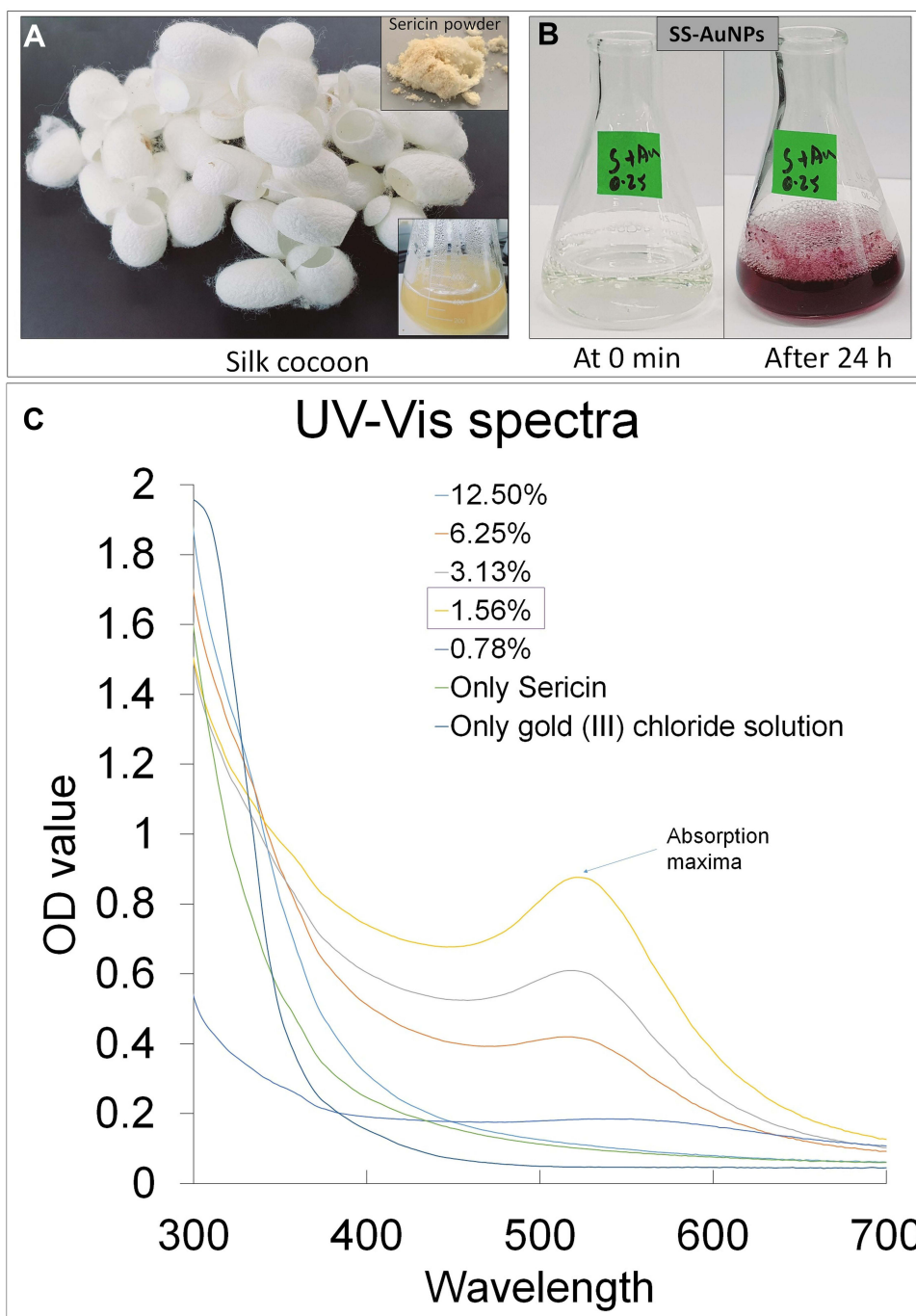


Figure 1 (A) Silk cocoon, sericin powder, and sericin solution; (B) Color change during biosynthesis of SSP-AuNPs; (C) UV-VIS spectral analysis of SSP-AuNPs at different sericin concentrations.

the synthesized NPs with better colloidal nature.^{37,48} Further, it is said that the high positive or negative values of the zeta potential showed a tendency to repel each other among the nanoparticles and thus reduce the accumulation of the NPs among each other.⁴⁹ Here, the polydispersed nature of the SSP-AuNPs is mainly because of the high negative zeta potential which averts the aggregation of the NPs among each other, resulting in well dispersed and stable materials. The current hypothesis is also proved by the TEM image (Figure 2A).

Further, to study the crystalline nature of the SSP-AuNPs, the XRD analysis was performed and the results are shown in Figure 4. The five well-defined diffraction peaks were detected at 2 theta angles in the SSP-AuNPs at 38.3°, 44.47°, 64.73°, 77.43°, and 82.33°.

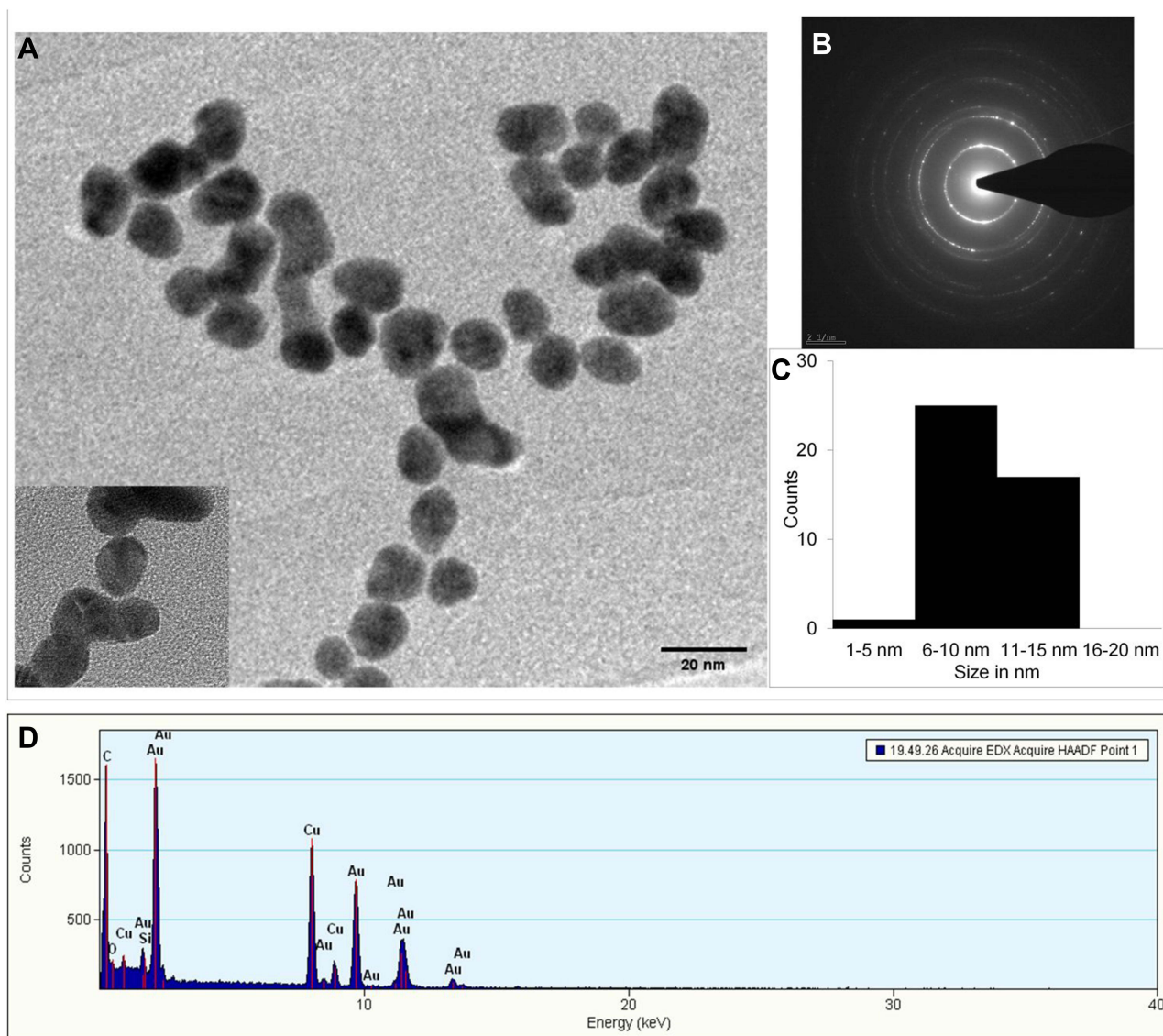


Figure 2 (A) TEM image of SSP-AuNPs (inset: magnified view); (B) SAED images of SSP-AuNPs; (C) size distribution; (D) EDS spectra of the SSP-AuNPs.

64.96°, 77.93°, and 82.21° which are assigned to 111, 200, 220, 311, and 222 respectively as per the Bragg's reflections of the FCC crystalline gold structure in accordance with JCPDs Card No. 65–8601.^{44,50} The distinctly broad diffraction peaks of the SSP-AuNPs indicate the small size of the synthesized NPs. It is remarkable here that the peak at 38.3° corresponding to (111), is more intense than that of the other planes^{51,52} which was observed in the XRD profile and it confirms that the obtained SSP-AuNPs were crystalline in nature (Figure 4). These obtained results corroborate with previously reported results.^{53–55} Apart from the distinct peaks, few other peaks were observed (denoted as “*” in the Figure 4), and among them, two peaks between 20° and 30° 2 theta angle might be due to the presence of different amino acids in the sericin.⁵⁰

To identify the major functional groups present in the SSP and SSP-AuNPs, the FT-IR analysis was carried out. The FTIR spectrum of the SSP was found as 3375.08 cm⁻¹, 1658.45, 701.19, 668.27, and 598.00 cm⁻¹. Whereas in the case of the SSP-AuNPs, the spectrums were probably shifted to 3345.59, 1643.51, 665.12, 597.85, and 554.23 cm⁻¹, respectively (Figure 5). In the FT-IR spectra of the SSP-AuNPs, the significant peaks of pure silk sericin were conserved, which signifies the successful capping of sericin on the SSP-AuNPs.³⁰ The FTIR results showed a variation in peak values with changed stretching modes between SSP to SSP-AuNPs (Figure 5). For SSP-AuNPs, the detected peaks at 3345.59 cm⁻¹

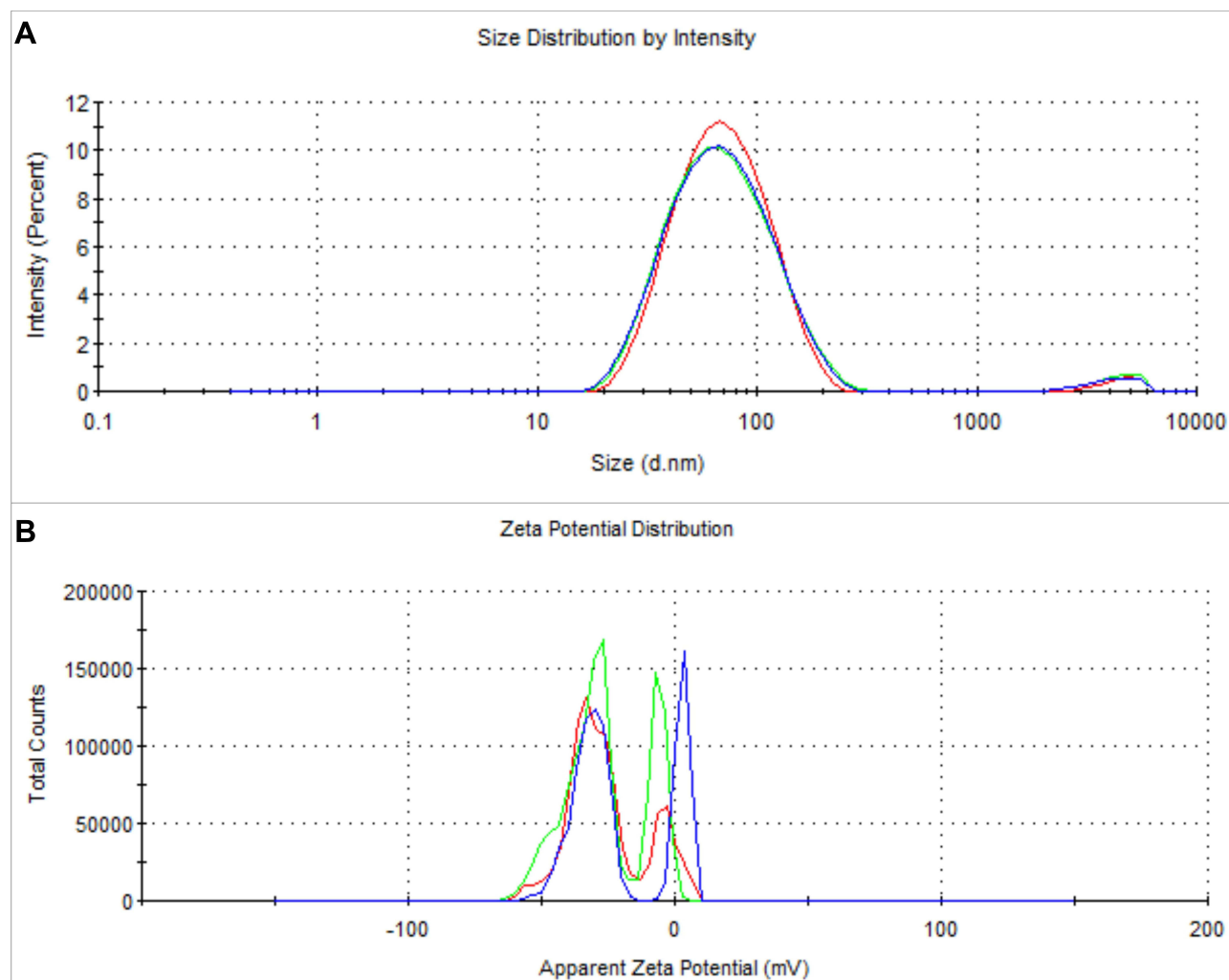


Figure 3 (A) Particle size distribution and (B) zeta potential of SSP-AuNPs.

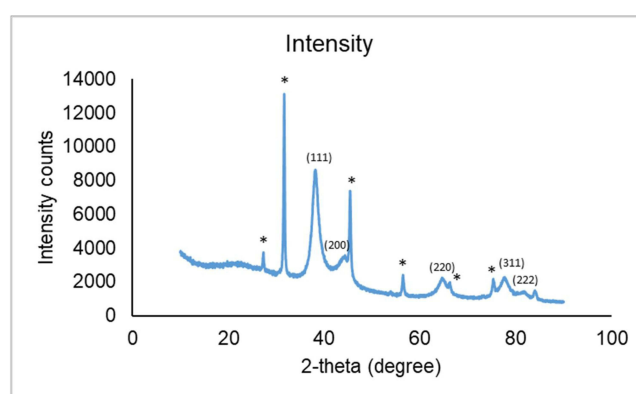


Figure 4 XRD analysis of the biosynthesized SSP-AuNPs. *Denotes some unknown peaks.

may be due to the O-H stretch, H-bonded bond of alcohols and phenols, or due to the N-H stretch of the primary and secondary amines and amides functional groups.⁵⁶ The peaks at 1643.51 cm^{-1} state the presence of medium – C=C-stretch bond of alkenes or N-H stretch of the primary amines functional group. In the synthesis of SSP-AuNPs, amine groups might have played a major role as both the reducing agents and stabilizers due to the transmission of their

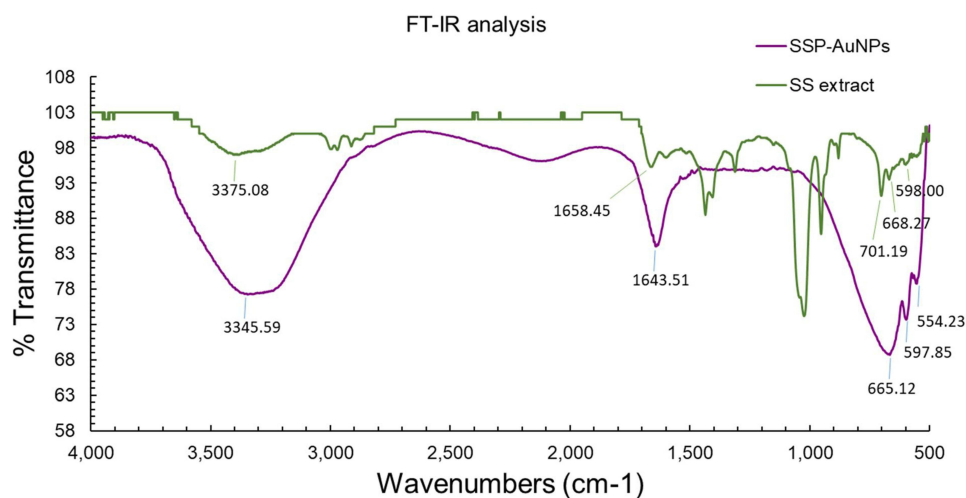


Figure 5 FT-IR analysis of the biosynthesized SSP-AuNPs and the SSP extract.

electrons to the Au^{3+} ions.³⁰ The peaks at 597.85 cm^{-1} and 554.33 cm^{-1} specify the existence of the C-Br stretch bond, which belongs to the alkyl halide functional groups.⁵⁶ This observation suggested that the N-H and -C=C- functional groups in the SSP must have supported the formation of the SSP-AuNPs.³⁰ The shifting of different functional groups from the SSP-AuNPs to SSP-AuNPs might be due to the progression of the synthesis process. It is also found that, when both the spectra are compared, a clear peak at 554.23 has appeared in the SSP-AuNPs which could be due to the capping and the stabilization of the SSP-AuNPs by the SSP. It was believed that the interactions of the hydroxyl groups of SSP with the Au^{3+} ions could have circumvented the agglomeration and precipitation of SSP-AuNPs in the high ionic strength solutions.^{30,57}

The TG/DTG analysis of the SSP-AuNPs at $25\text{ }^{\circ}\text{C}$ – $990\text{ }^{\circ}\text{C}$ is presented in [Figure 6A](#). The TG/DTG displayed a total weight decomposition of 66.81% in three phases ([Figure 6A](#)). The first phase of decomposition was from 25 to $150\text{ }^{\circ}\text{C}$ that accounts for 6.71% of weight loss which could be due to the water and other small molecules attached to the surface of the particles and resulting in a small amount of mass loss of the sample; the second phase was from 151 to $450\text{ }^{\circ}\text{C}$, accounting for 50.40% of the weight decomposition and due to the loss of organic materials in the sample and as the temperature further continues to rise, the third phase was from $451\text{ }^{\circ}\text{C}$ onwards, that accounts for a weight loss of around 9.70% and that might be due to the degradation of the residual compounds present in the sample. With the increase in temperature, the DTG curve shows five peaks, and the inflection points of the peaks are $99.9\text{ }^{\circ}\text{C}$, $143.0\text{ }^{\circ}\text{C}$, $220.0\text{ }^{\circ}\text{C}$, $314.5\text{ }^{\circ}\text{C}$, and $394.5\text{ }^{\circ}\text{C}$, respectively ([Figure 6A](#)). The reduction in the weight of the synthesized SSP-AuNPs signifies the involvement of the sericin protein in the biosynthesis, capping, and stabilization of the nanoparticles.^{58–61}

The shape and size of the SSP-AuNPs were further determined by the AFM analysis in both 2D and 3D ([Figure 6B and C](#)). [Figure 6B](#) represents the two-dimensional image of SSP-AuNPs which are monodispersed and spherical in shape. [Figure 6C](#) represents the three-dimensional images of SSP-AuNPs are crystalline and spherical in shape. The height measurement showed that the SSP-AuNPs had a diameter of around 10 nm. The current result corroborates with the previously published literature.^{61–63}

Biological Potential of the Biosynthesized SSP-AuNPs

The biological potential of the SSP-AuNPs was investigated by the wound-healing, antioxidant and antibacterial assays. The wound healing potential of the SSP-AuNPs was determined by the scratch wound assay, and the results are presented in [Figure 7](#). Prior to the analysis, the sample was subjected to cell viability (cytotoxicity) study, and the results showed that SSP-AuNPs have no influence on the cell viability of the keratinocytes with more than 94% viability percent at three different tested concentrations (5, 10 and $25\text{ }\mu\text{g/mL}$) ([Figure 7A](#)). The wound healing potential was estimated by visualizing the closure of the scratch produced after 12 and 24 hours of incubation and the results were compared

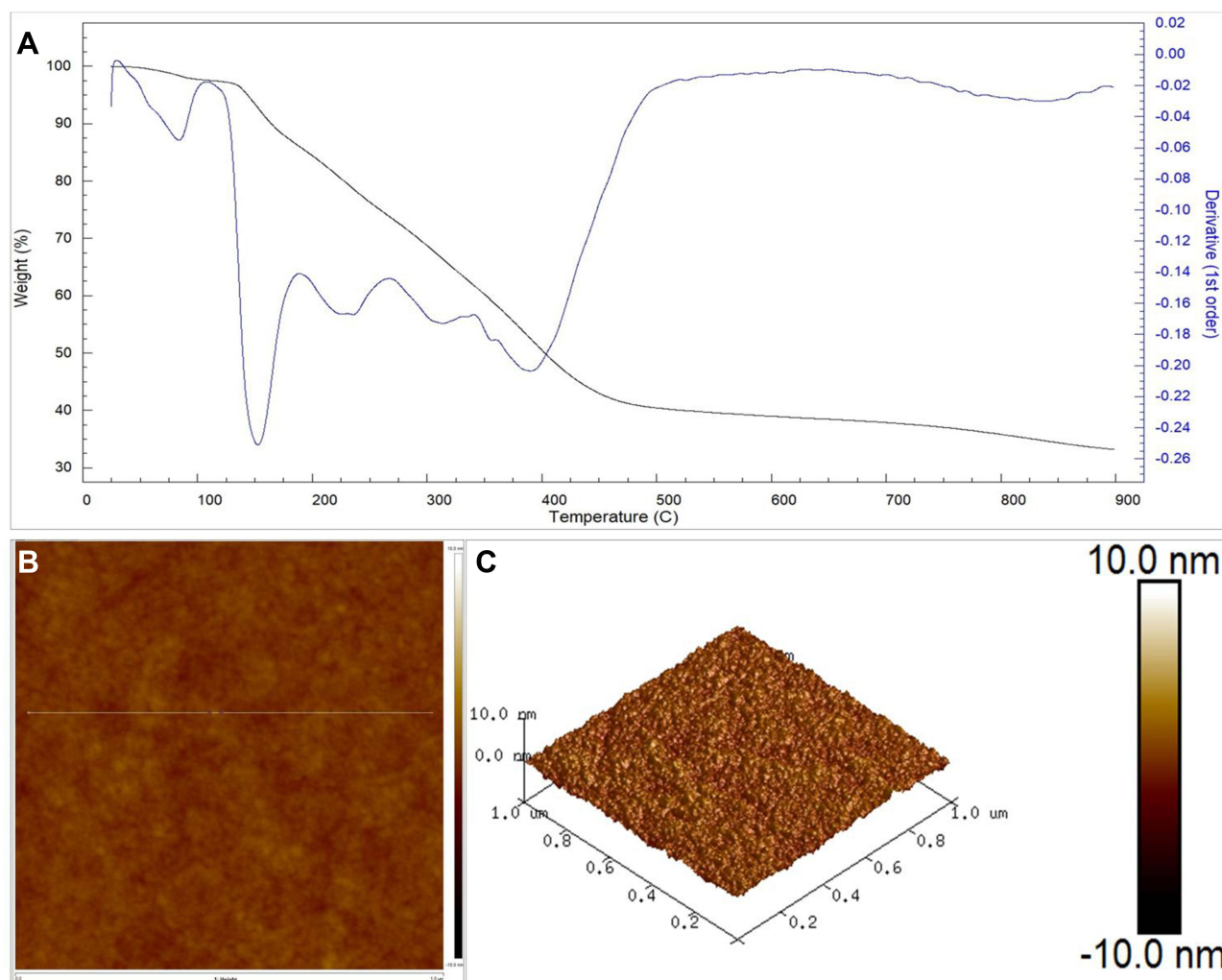


Figure 6 (A) TG/DTG analysis of the biosynthesized SSP-AuNPs; and AFM analysis of the biosynthesized SSP-AuNPs (B) 2D image and (C) 3D image.

with the results of *Centella asiatica*, taken as the positive control (Figure 7B). The results showed that the SSP-AuNPs promote wound healing without having no influence on cell viability. However, the highest concentration of the SSP-AuNPs (25 $\mu\text{g/mL}$) did not have the desired impact of increasing wound healing. Besides, the wound closure rate was also calculated and results showed that the SSP-AuNPs (5 and 10 $\mu\text{g/mL}$) exhibited promising wound closure rates of 70.96 and 69.76% respectively as compared to 74.91% by the *Centella asiatica* taken as the positive control (Figure 7C).

Wound healing is a complex and vigorous process that is a reaction to the cell injury intended at restructuring the damaged tissue and involves particular management of the angiogenesis, connective tissue repair, and re-epithelialization.^{64,65} It has been testified that the wound healing activity of any tested drugs is accredited mainly to the enhanced wound contraction and the shorter epithelialization period.^{64,66} The keratinocytes are the numerous cells of the epidermis of the skin and are commonly used as the cells for the wound healing experiment. They play a crucial role in the wound healing progression, principally in the proliferation phase that includes the re-epithelialization and granulation of tissue.^{34,67} Increased keratinocyte proliferation and migration are two mechanisms that contribute to wound healing. The efficacy of SSP-AuNPs in boosting wound healing is likely owing to their enhanced migration, as determined by the cell viability test. *C. asiatica* extract was employed as a positive control in this experiment since it is well known for its wound-healing qualities.³⁴

The antioxidant potential of the SSP-AuNPs was investigated by the DPPH, ABTS, and the reducing power assay, and the results are presented in Figure 8. The biosynthesized SSP-AuNPs exhibited overall a good DPPH scavenging

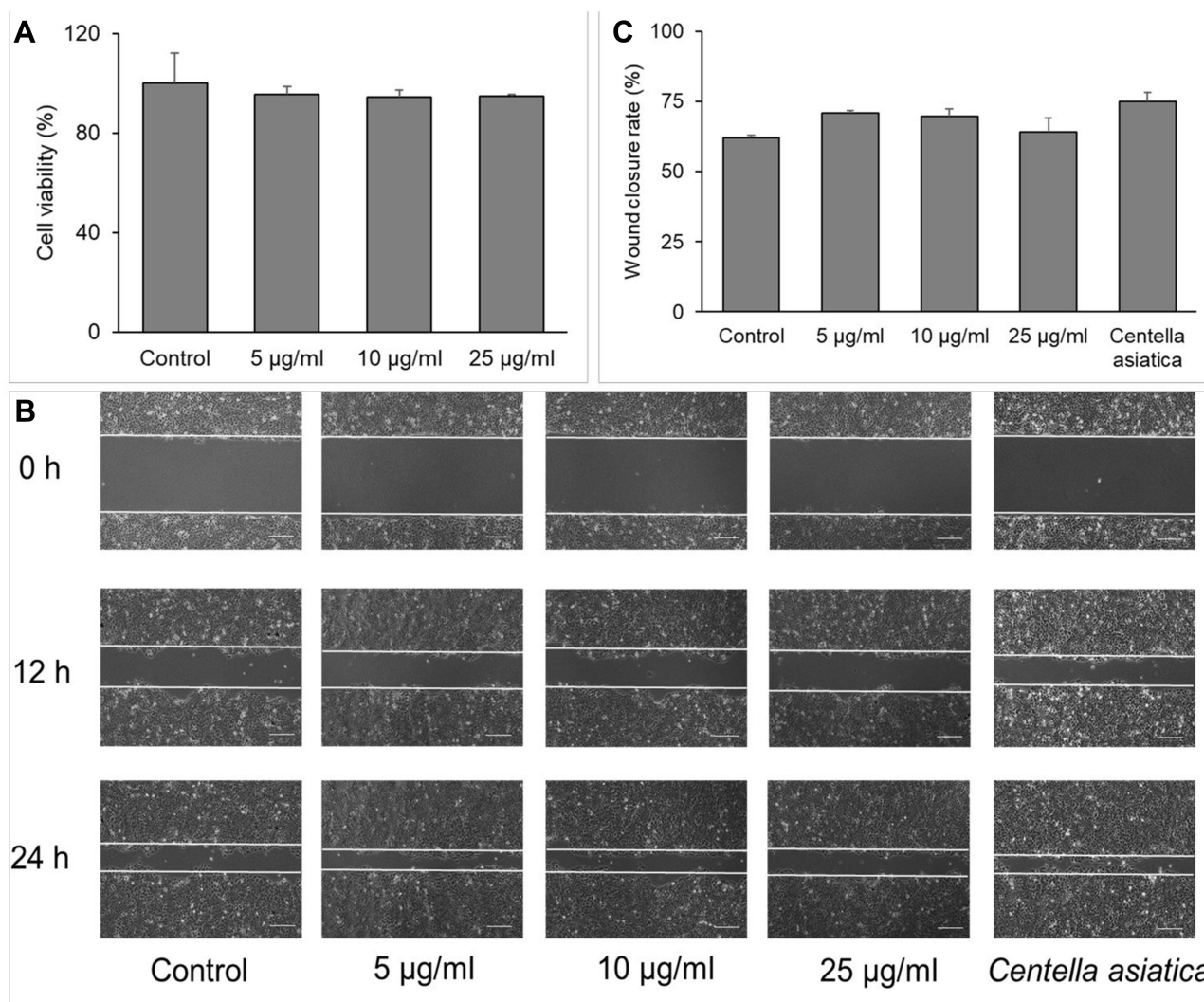


Figure 7 Wound healing potential of SSP-AuNPs. (A) Cell viability test; (B) Scratch wound assay images at 0 h, 12 h, and 24 h of incubation; and (C) Wound closure rate.

potential and all the three tested concentrations of 25, 50, and 100 µg/mL as compared to the BHT, taken as the reference standard compound (Figure 8A). In fact, the SSP-AuNPs displayed a promising 74.37% of scavenging as compared to the 59.59% by BHT at 100 µg/mL concentration (Figure 8A). Similarly, it also displayed a moderate ABTS free radical scavenging potential at the three concentrations as compared to the standard BHT (Figure 8B). The maximum scavenging potential of 26.56% was exhibited at 100 µg/mL concentration in comparison to 91.71% by BHT at the same concentration. Again, the SSP-AuNPs displayed an increasing reducing power at all three different tested concentrations and the results are comparable with the standard BHT, taken as the reference compound (Figure 8C). Further, the IC₅₀ values of the SSP-AuNPs for the three antioxidant assays are also calculated, and the results are presented in Table 1. The IC₅₀ values of the SSP-AuNPs for the DPPH assay were found to be 68.48 µg/mL; for ABTS it is 173.43 µg/mL and for the reducing power, the IC_{0.5} value is 208.68 µg/mL (Table 1). Similarly, for the standard BHT, the IC₅₀ and the IC_{0.5} values were calculated as 50.80 µg/mL, 31.91 µg/mL, and 75.79 µg/mL for DPPH, ABTS, and reducing power assays respectively (Table 1). Besides, the total antioxidant capacity (TAC) of the SSP-AuNPs was evaluated, and the result is presented in Table 1). The TAC for SSP-AuNPs and BHT was calculated as 23.64 µM Trolox equivalent and 23.43 µM Trolox equivalent at 50 µg/mL concentration.

Overall, the SSP-AuNPs displayed a moderate antioxidant potential and the activity might be due to the sericin protein used as the reducing and capping agent in the synthesis of SSP-AuNPs. The results also showed that the SSP-

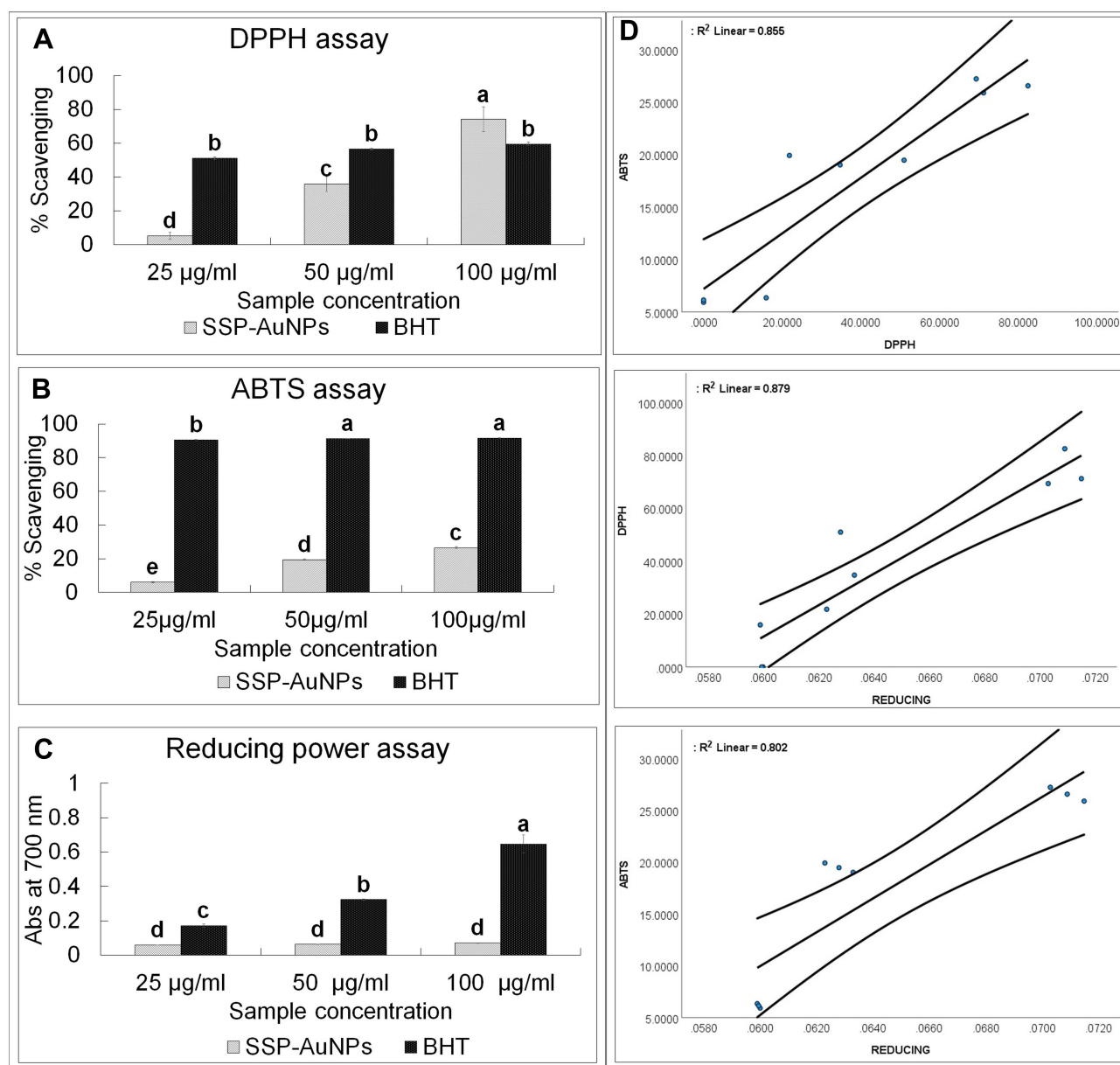


Figure 8 Antioxidant scavenging potential of the biosynthesized SSP-AuNPs. (A) DPPH free radical scavenging assay; (B) ABTS free radical scavenging assay; (C) Reducing power assay; (D) Regression analysis of antioxidant parameters. Different superscript letters (a–e) in each bar of the figure A–C respectively are statistically significant at $P < 0.05$.

AuNPs exhibited potent free radical scavenging activities that increased with the increase in the concentration of the sample, which might be due to their ability to donate electrons or hydrogen ions to the free radicals to neutralize them.^{68,69} The excess production of the extremely reactive, unsteady, and initiator of the free radical reactions because of the disparity between the oxidation-reduction process resulted in the generation of cell stress and cell death-related ailments.^{49,70} Hence, it is very much essential to neutralize the effect of the free radicals, which in this case can be effectively carried out by the SSP-AuNPs. When the antioxidant parameters are plotted against each other, a positive tendency was observed between them the R^2 values of 0.855 (for DPPH-ABTS), 0.879 (for DPPH-reducing), and 0.802 (for ABTS-reducing) (Figure 8D). Similarly, a strong positive trend was also observed from the Pearson's correlation plot between the DPPH, ABTS, and the reducing power assays with an r -value of 0.924, 0.938, and 0.895 respectively at $P < 0.01$ (Table 2).

Table 1 IC₅₀ Values of Antioxidant Assays and Total Antioxidant Capacity of SSP-AuNPs

Antioxidant Assays	IC ₅₀ value (µg/mL)	
	SSP-AuNPs	BHT
DPPH	68.48	50.80
ABTS	173.43	31.91
Reducing (IC _{0.5})	208.68	75.79
TAC* (µM Trolox equivalent)	23.64±4.07	23.43±6.99

Note: *TAC value at 50 µg/mL of the sample.

Table 2 Correlation Analysis Between the Three-Antioxidant Parameters of SSP-AuNPs

Correlations			
	DPPH	ABTS	REDUCING
DPPH	1	0.924**	0.938**
ABTS		1	0.895**
REDUCING			1

Note: **Correlation is significant at the 0.01 level (2-tailed).

Table 3 Antibacterial Potential of SSP-AuNPs and Cephalexin Against the Pathogenic Bacteria

Pathogenic Bacteria	Antibacterial Activity in Diameter of Inhibition Zones (mm)		MIC and MBC			
			SSP-AuNPs		Cephalexin	
	SSP-AuNPs (100µg/disc)	Cephalexin (10µg/disc)	MIC (µg/mL)	MBC (µg/mL)	MIC (µg/mL)	MBC (µg/mL)
<i>E. coli</i>	11.10±0.58 ^{e*}	13.12±0.16 ^c	50	100	2.5	05
<i>E. faecium</i>	12.39±0.04 ^d	13.24±0.48 ^c	25	50	2.5	05
<i>S. enterica</i>	14.20±0.41 ^b	12.45±0.67 ^d	25	50	05	10
<i>S. Typhimurium</i>	14.96±0.08 ^a	12.08±0.39 ^d	25	50	05	10

Notes: *All data are expressed in mm as mean value ± standard deviation. Diameter of inhibition zones with different superscript letters (a–e) in both the columns are statistically significant at P<0.05.

At last, the antibacterial potential of the biosynthesized SSP-AuNPS was estimated against four different foodborne pathogenic bacteria, and the result is presented as the diameter of inhibition zones (Table 3, Figure 9). The results displayed that SSP-AuNPs at a concentration of 100 µg/disc, are highly effective against the four tested pathogens with the diameter of inhibition zones ranging between 11.10 and 14.96 mm as compared to the 12.08–13.24 mm by the cephalixin (at 10 µg/disc), taken as the positive control (Table 3, Figure 9). The SSP-AuNPs were more active against the *S. Typhimurium* with 14.96 mm inhibition zones, whereas the cephalixin displayed 12.08 mm against the same pathogen (Table 3, Figure 9). The MIC and MBC of the SSP-AuNPs and the cephalixin ranged between 25–100 µg/mL and 2.5–10 µg/mL, respectively (Table 3).

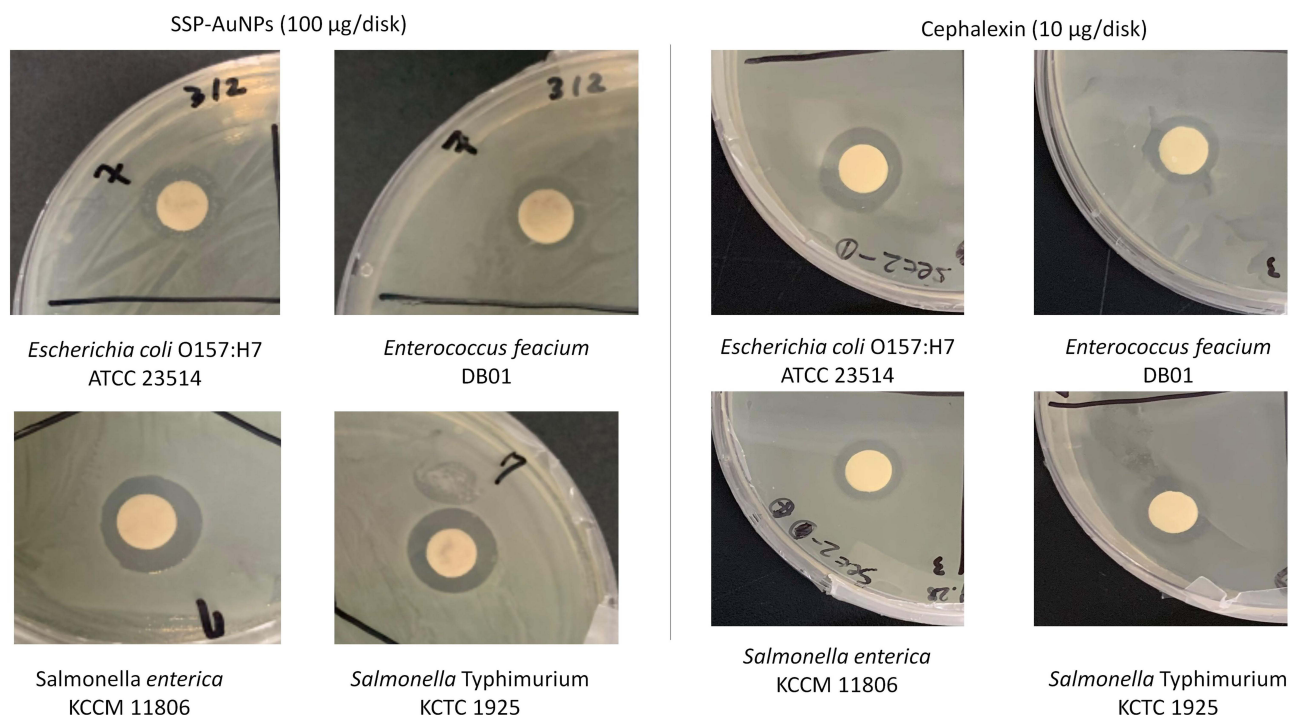


Figure 9 Antibacterial potential of the biosynthesized SSP-AuNPs against the tested pathogenic bacteria.

Currently, the emergence of multidrug-resistant pathogens in the environment is very common, and it might have a hostile effect on human health.^{71,72} There are a few hypotheses, predicting the antibacterial mode of action of the SSP-AuNPs against the four tested foodborne pathogenic bacteria. One of them is that its antibacterial effects could be credited to their ability to attach to the cell wall of the pathogenic bacteria and causing cavity and altering the permeability of the bacterial cell membrane and resulting in the death of the bacterial cells as evident from the previously published literature.^{73,74} Besides, another hypothesis on the antibacterial mode of action of the SSP-AuNPs against the four tested foodborne pathogenic bacteria could be that, the SSP-AuNPs might have easily infiltrated into the bacterial cell wall due to their smaller size and spherical shapes and eventually could have damaged the cell wall, resulting in the outflow of the cellular material and cell death.^{33,75} The third one is that the SSP-AuNPs could have bound to the bacterial DNA, resulting in the inhibition of uncoiling and transcription of the bacterial DNA, which leads to the leading to cell death.⁷⁵ This entire hypothesis confirms that the SSP-AuNPs could serve as a promising antibacterial agent in various applications in the food, cosmetics, and biomedical industries.

Conclusion

The sericin protein-based biosynthesis of the SSP-AuNPs in the presence of the UV radiations could be an alternative, cost-effective and easy method of gold nanoparticle biosynthesis that could replace the conventional chemical methods. The use of sericin protein which is usually a bioproduct of the sericulture industry, as a reducing and capping agent in the biosynthesis process is an addition to the eco-friendly and economical way of synthesizing nanoparticles and also utilization of biological waste materials from the sericulture industries. The synthesized SSP-AuNPs were characterized by a number of techniques and the visual color change and UV-Vis spectroscopy confirmed the synthesis of gold nanoparticles, with absorption maxima at 508 nm. The average size by the particle size analyzer was determined as 54.82 nm and the zeta potential is -19.8 mV. The SSP-AuNPs displayed as a promising candidate in the healing of skin cells related wounds at a concentration of 5 and 10 µg/mL, scavenger of free radicals proving its antioxidant capacity (around 74.37% of scavenging as compared to 59.59% by the BHT at 100 µg/mL concentration) and inhibition of pathogenic bacteria as a strong antibacterial component (with a diameter of inhibition zones ranging between 11.10 and

14.96 mm as compared to 12.08–13.24 mm by the positive control cephalexin). Overall, the SSP-AuNPs could be an encouraging candidate for food cosmetics, and biomedical industries in applications such as a component of wound healing drugs, antioxidant components in skin care, and antibacterial components in antibacterial bandages and ointments. These sericin-mediated SSP-AuNPs can be a favorable nanoscale-sized mediator for biomedical applications with their in vitro biocompatibility, admirable aqueous stability and efficient wound healing, antioxidant and antibacterial activities.

Acknowledgments

All authors are grateful to their respective institutions for their support. This work was supported by the National Research Foundation of Korea (NRF) grant funded by the Korea government (MSIT) (No. 2020R1G1A1004667), the Republic of Korea.

Funding

This work was supported by the National Research Foundation of Korea (NRF) grant funded by the Korea government (MSIT) (No. 2020R1G1A1004667), the Republic of Korea.

Disclosure

The authors declare that there is no conflict of interest exists with this manuscript.

References

- Balasubramanian S, Kala SMJ, Pushparaj TL, Kumar P. Biofabrication of gold nanoparticles using *Cressa cretica* leaf extract and evaluation of catalytic and antibacterial efficacy. *Nano Biomed Eng.* 2019;11(1):58–66. doi:10.5101/nbe.v11i1.p58-66
- Ocsoy I, Tasdemir D, Mazicioglu S, Celik C, Kati A, Ulgen F. Biomolecules incorporated metallic nanoparticles synthesis and their biomedical applications. *Mater Lett.* 2018;212:45–50. doi:10.1016/j.matlet.2017.10.068
- Balasubramanian S, Kala SMJ, Pushparaj TL. Biogenic synthesis of gold nanoparticles using *Jasminum auriculatum* leaf extract and their catalytic, antimicrobial and anticancer activities. *J Drug Deliv Sci Technol.* 2020;57:101620. doi:10.1016/j.jddst.2020.101620
- Ma X, Zhao Y, Liang X-J. Theranostic nanoparticles engineered for clinic and pharmaceuticals. *Acc Chem Res.* 2011;44(10):1114–1122. doi:10.1021/ar2000056
- Shrivastava K, Wu H-F. Multifunctional nanoparticles composite for MALDI-MS: Cd²⁺-doped carbon nanotubes with CdS nanoparticles as the matrix, preconcentrating and accelerating probes of microwave enzymatic digestion of peptides and proteins for direct MALDI-MS analysis. *J Mass Spectrom.* 2010;45(12):1452–1460. doi:10.1002/jms.1861
- Maruyama T, Fujimoto Y, Maekawa T. Synthesis of gold nanoparticles using various amino acids. *J Colloid Interface Sci.* 2015;447:254–257. doi:10.1016/j.jcis.2014.12.046
- Akhtar MS, Panwar J, Yun Y-S. Biogenic synthesis of metallic nanoparticles by plant extracts. *ACS Sustain Chem Eng.* 2013;1(6):591–602. doi:10.1021/sc300118u
- Shin M, Yang S, Kwak HW, Lee KH. Synthesis of gold nanoparticles using silk sericin as a green reducing and capping agent. *Eur Polym J.* 2022;164:110960. doi:10.1016/j.eurpolymj.2021.110960
- Liz-Marzán LM. Tailoring surface plasmons through the morphology and assembly of metal nanoparticles. *Langmuir.* 2006;22(1):32–41. doi:10.1021/la0513353
- Shivananda C, Asha S, Madhukumar R, et al. Biosynthesis of colloidal silver nanoparticles: their characterization and antibacterial activity. *Biomed Phys Eng Express.* 2016;2(3):035004. doi:10.1088/2057-1976/2/3/035004
- Lakshmeesha Rao B, Gowda M, Asha S, et al. Rapid synthesis of gold nanoparticles using silk fibroin: characterization, antibacterial activity, and anticancer properties. *Gold Bull.* 2017;50(4):289–297. doi:10.1007/s13404-017-0218-8
- Parushuram N, Asha S, Suma S, Krishna K, Neelakandan R, Sangappa Y. Green synthesis of high yield mono-dispersed gold nanoparticles using silk-sericin and characterization. Paper presented at: AIP Conference Proceedings; 2019.
- Abirami M, Shayanthi SS, Rajendran R. Synthesis and characterization of PVA based sericin film for antibacterial wound dressing. *Int J Pharm Sci Res.* 2019;10:875–880.
- Su D, Ding S, Shi W, Huang X, Jiang L. *Bombyx mori* silk-based materials with implication in skin repair: sericin versus regenerated silk fibroin. *J Biomater Appl.* 2019;34(1):36–46. doi:10.1177/0885328219844978
- Saravanan A, Huang B-R, Kathiravan D, Prasannan A. Natural biowaste-cocoon-derived granular activated carbon-coated ZnO nanorods: a simple route to synthesizing a core-shell structure and its highly enhanced UV and hydrogen sensing properties. *ACS Appl Mater Interfaces.* 2017;9(45):39771–39780. doi:10.1021/acsami.7b11051
- Barajas-Gamboa JA, Serpa-Guerra AM, Restrepo-Osorio A, Álvarez-López C. Sericin applications: a globular silk protein. *Ingeniería y competitividad.* 2016;18(2):193–206. doi:10.25100/iyc.v18i2.2167
- Gulrajani M. Sericin: a Bio-molecule of value. Paper presented at: Souveni 20th Congress of the International Sericultural Commission Bangalore, India 15–18th December 2005; 2005.
- Fabiani C, Pizzichini M, Spadoni M, Zedda G. Treatment of waste water from silk degumming processes for protein recovery and water reuse. *Desalination.* 1996;105(1–2):1–9. doi:10.1016/0011-9164(96)00050-1

19. Kunz RI, Brancalhão RMC, Ribeiro L, Natali MRM. Silk worm sericin: properties and biomedical applications. *Biomed Res Int.* 2016;2016. doi:10.1155/2016/8175701
20. Kundu SC, Dash BC, Dash R, Kaplan DL. Natural protective glue protein, sericin bioengineered by silkworms: potential for biomedical and biotechnological applications. *Prog Polym Sci.* 2008;33(10):998–1012. doi:10.1016/j.progpolymsci.2008.08.002
21. Mondal M, Trivedy K, Nirmal KS. The silk proteins, sericin and fibroin in silkworm, *Bombyx mori* Linn.,-a review. *Casp J Environ Sci.* 2007;5(2):63–76.
22. Shao Z, Vollrath F. Surprising strength of silkworm silk. *Nature.* 2002;418(6899):741. doi:10.1038/418741a
23. Kumar JP, Mandal BB. Silk sericin induced pro-oxidative stress leads to apoptosis in human cancer cells. *Food Chem Toxicol.* 2019;123:275–287. doi:10.1016/j.fct.2018.10.063
24. Chlapanidas T, Faragò S, Lucconi G, et al. Sericins exhibit ROS-scavenging, anti-tyrosinase, anti-elastase, and in vitro immunomodulatory activities. *Int J Biol Macromol.* 2013;58:47–56. doi:10.1016/j.ijbiomac.2013.03.054
25. Saha J, Mondal M, Karim Sheikh M, Habib M. Extraction, structural and functional properties of silk sericin biopolymer from *Bombyx mori* silk cocoon waste. *J Text Sci Eng.* 2019;9(01):2. doi:10.4172/2165-8064.1000390
26. Miguel GA, Álvarez-López C. Extraction and antioxidant activity of sericin, a protein from silk. *Braz J Food Technol.* 2020;23. doi:10.1590/1981-6723.05819
27. Wang Z, Zhang Y, Zhang J, et al. Exploring natural silk protein sericin for regenerative medicine: an injectable, photoluminescent, cell-adhesive 3D hydrogel. *Sci Rep.* 2014;4(1):1–11.
28. Veiga A, Castro F, Rocha F, Oliveira AL. Recent advances in silk sericin/calcium phosphate biomaterials. *Front Mater.* 2020;7:24.
29. Jena K, Pandey J, Kumari R, Sinha A, Gupta V, Singh G. Free radical scavenging potential of sericin obtained from various ecoraces of tasar cocoons and its cosmeceuticals implication. *Int J Biol Macromol.* 2018;120:255–262. doi:10.1016/j.ijbiomac.2018.08.090
30. Akturk O, Gun Gok Z, Erdemli O, Yigitoglu M. One-pot facile synthesis of silk sericin-capped gold nanoparticles by UVC radiation: investigation of stability, biocompatibility, and antibacterial activity. *J Biomed Mater Res A.* 2019;107(12):2667–2679. doi:10.1002/jbm.a.36771
31. Iravani S, Korbekandi H, Mirmohammadi SV, Zolfaghari B. Synthesis of silver nanoparticles: chemical, physical and biological methods. *Res Pharm Sci.* 2014;9(6):385.
32. Iravani S, Zolfaghari B. Green synthesis of silver nanoparticles using *Pinus eldarica* bark extract. *Biomed Res Int.* 2013;2013. doi:10.1155/2013/639725
33. Patra JK, Baek K-H. Novel green synthesis of gold nanoparticles using *Citrullus lanatus* rind and investigation of proteasome inhibitory activity, antibacterial, and antioxidant potential. *Int J Nanomedicine.* 2015;10:7253. doi:10.2147/IJN.S95483
34. Nguyen LTH, Ahn S-H, Choi M-J, Yang I-J, Shin H-M. Puerarin improves dexamethasone-impaired wound healing in vitro and in vivo by enhancing keratinocyte proliferation and migration. *Appl Sci.* 2021;11(19):9343. doi:10.3390/app11199343
35. Su L, Fu L, Li X, et al. Loss of CAR promotes migration and proliferation of HaCaT cells, and accelerates wound healing in rats via Src-p38 MAPK pathway. *Sci Rep.* 2016;6:19735. doi:10.1038/srep19735
36. Patra JK, Kim SH, Baek K-H. Antioxidant and free radical-scavenging potential of essential oil from *Enteromorpha linza* L. Prepared by microwave-assisted hydrodistillation. *J Food Biochem.* 2015;39(1):80–90. doi:10.1111/jfbc.12110
37. Das G, Shin HS, Patra JK. Multitherapeutic efficacy of curly kale extract fabricated biogenic silver nanoparticles. *Int J Nanomedicine.* 2022;17:1125–1137. doi:10.2147/IJN.S308478
38. Patra JK, Kim SH, Hwang H, Choi JW, Baek K-H. Volatile compounds and antioxidant capacity of the bio-oil obtained by pyrolysis of Japanese Red Pine (*Pinus densiflora* Siebold and Zucc.). *Molecules.* 2015;20(3):3986–4006. doi:10.3390/molecules20033986
39. Kubo I, Fujita K-I, Kubo A, Nihei K-I, Ogura T. Antibacterial activity of coriander volatile compounds against *Salmonella choleraesuis*. *J Agric Food Chem.* 2004;52(11):3329–3332. doi:10.1021/jf0354186
40. Harisha K, Parushuram N, Asha S, Suma S, Narayana B, Sangappa Y. Eco-synthesis of gold nanoparticles by Sericin derived from *Bombyx mori* silk and catalytic study on degradation of methylene blue. *Part Sci Technol.* 2021;39(2):131–140. doi:10.1080/02726351.2019.1666951
41. Joshi P, Shewale V, Pandey R, Shanker V, Hussain S, Karnia SP. Tryptophan-gold nanoparticle interaction: a first-principles quantum mechanical study. *J Phys Chem C.* 2011;115(46):22818–22826. doi:10.1021/jp2070437
42. Michałowska A, Krajczewski J, Kudelski A. Magnetic iron oxide cores with attached gold nanostructures coated with a layer of silica: an easily, homogeneously deposited new nanomaterial for surface-enhanced Raman scattering measurements. *Spectrochimica Acta Part A.* 2022;277:121266. doi:10.1016/j.saa.2022.121266
43. Sathiyaraj S, Suriyakala G, Gandhi AD, et al. Biosynthesis, characterization, and antibacterial activity of gold nanoparticles. *J Infect Public Health.* 2021;14(12):1842–1847. doi:10.1016/j.jiph.2021.10.007
44. Das J, Velusamy P. Catalytic reduction of methylene blue using biogenic gold nanoparticles from *Sesbania grandiflora* L. *J Taiwan Inst Chem Eng.* 2014;45(5):2280–2285. doi:10.1016/j.jtice.2014.04.005
45. Mahakham W, Theerakulpisut P, Maensiri S, Phumying S, Sarmah AK. Environmentally benign synthesis of phytochemicals-capped gold nanoparticles as nanopriming agent for promoting maize seed germination. *Sci Total Environ.* 2016;573:1089–1102. doi:10.1016/j.scitotenv.2016.08.120
46. Princy K, Gopinath A. Optimization of physicochemical parameters in the biofabrication of gold nanoparticles using marine macroalgae *Padina tetraströmatica* and its catalytic efficacy in the degradation of organic dyes. *J Nanostructure Chem.* 2018;8(3):333–342. doi:10.1007/s40097-018-0277-2
47. Pyrz WD, Buttrey DJ. Particle size determination using TEM: a discussion of image acquisition and analysis for the novice microscopist. *Langmuir.* 2008;24(20):11350–11360. doi:10.1021/la801367j
48. Singh H, Du J, Yi T-H. Green and rapid synthesis of silver nanoparticles using *Borago officinalis* leaf extract: anticancer and antibacterial activities. *Artif Cells, Nanomed Biotechnol.* 2017;45(7):1310–1316. doi:10.1080/21691401.2016.1228663
49. Sharma A, Sagar A, Rana J, Rani R. Green synthesis of silver nanoparticles and its antibacterial activity using fungus *Talaromyces purpureogenus* isolated from *Taxus baccata* Linn. *Micro Nano Systems Letters.* 2022;10(1):1–12. doi:10.1186/s40486-022-00144-9
50. Yang C, Chen S, Su H, et al. Biocompatible, small-sized and well-dispersed gold nanoparticles regulated by silk fibroin fiber from *Bombyx mori* cocoons. *Front Mater Sci.* 2019;13(2):126–132. doi:10.1007/s11706-019-0456-1

51. Borhamdin S, Shamsuddin M, Alizadeh A. Biostabilised icosahedral gold nanoparticles: synthesis, cyclic voltammetric studies and catalytic activity towards 4-nitrophenol reduction. *J Exp Nanosci.* 2016;11(7):518–530. doi:10.1080/17458080.2015.1090021
52. Lim SH, Ahn E-Y, Park Y. Green synthesis and catalytic activity of gold nanoparticles synthesized by *Artemisia capillaris* water extract. *Nanoscale Res Lett.* 2016;11(1):1–11. doi:10.1186/s11671-016-1694-0
53. Suchomel P, Kvitěk L, Prucek R, et al. Simple size-controlled synthesis of Au nanoparticles and their size-dependent catalytic activity. *Sci Rep.* 2018;8(1):1–11. doi:10.1038/s41598-018-22976-5
54. Lin S, Lin X, Shang Y, Han S, Hasi W, Wang L. Self-assembly of faceted gold nanocrystals for surface-enhanced Raman scattering application. *J Phys Chem C.* 2019;123(40):24714–24722. doi:10.1021/acs.jpcc.9b06686
55. Hang NTN, Yang Y, Nam NQT, et al. Controlled synthesis of au nanoparticles by modified polyol methods: determination of their size, shape, and crystal structure. *Crystals.* 2021;11(11):1297. doi:10.3390/cryst11111297
56. Kalaiyarasu T, Karthi N, Sharmila GV, Manju V. In vitro assessment of antioxidant and antibacterial activity of green synthesized silver nanoparticles from *Digitaria radicata* leaves. *Asian J Pharm Clin Res.* 2016;9(1):1–6.
57. Aramwit P, Bang N, Ratanavaraporn J, Ekgasit S. Green synthesis of silk sericin-capped silver nanoparticles and their potent anti-bacterial activity. *Nanoscale Res Lett.* 2014;9(1):79. doi:10.1186/1556-276X-9-79
58. Patra JK, Baek K-H. Comparative study of proteasome inhibitory, synergistic antibacterial, synergistic anticandidal, and antioxidant activities of gold nanoparticles biosynthesized using fruit waste materials. *Int J Nanomed.* 2016;11:4691. doi:10.2147/IJN.S108920
59. Zhou L, Jiang C, Lin Q. Entropy analysis and grey cluster analysis of multiple indexes of 5 kinds of genuine medicinal materials. *Sci Rep.* 2022;12(1):6618. doi:10.1038/s41598-022-10509-0
60. Basavegowda N, Mishra K, Lee YR. Synthesis, characterization, and catalytic applications of hematite (α -Fe₂O₃) nanoparticles as reusable nanocatalyst. *Adv Natural Sci.* 2017;8(2):025017.
61. Hamelian M, Varmira K, Veisi H. Green synthesis and characterizations of gold nanoparticles using Thyme and survey cytotoxic effect, antibacterial and antioxidant potential. *J Photochem Photobiol B.* 2018;184:71–79. doi:10.1016/j.jphotobiol.2018.05.016
62. Hutchinson N, Wu Y, Wang Y, et al. Green synthesis of gold nanoparticles using upland cress and their biochemical characterization and assessment. *Nanomaterials.* 2022;12(1):28. doi:10.3390/nano12010028
63. Huang L, Tao K, Liu J, et al. Design and fabrication of multifunctional sericin nanoparticles for tumor targeting and pH-responsive subcellular delivery of cancer chemotherapy drugs. *ACS Appl Mater Interfaces.* 2016;8(10):6577–6585. doi:10.1021/acsami.5b11617
64. Kundu A, Ghosh A, Singh NK, et al. Wound healing activity of the ethanol root extract and polyphenolic rich fraction from *Potentilla fulgens*. *Pharm Biol.* 2016;54(11):2383–2393. doi:10.3109/13880209.2016.1157192
65. Wu X-B, Luo X-Q, Gu S-Y, Xu J-H. The effects of *Polygonum cuspidatum* extract on wound healing in rats. *J Ethnopharmacol.* 2012;141(3):934–937. doi:10.1016/j.jep.2012.03.040
66. Süntar IP, Akkol EK, Yilmazer D, et al. Investigations on the in vivo wound healing potential of *Hypericum perforatum* L. *J Ethnopharmacol.* 2010;127(2):468–477. doi:10.1016/j.jep.2009.10.011
67. Pastar I, Stojadinovic O, Tomic-Canic M. Role of keratinocytes in healing of chronic wounds. *Surg Technol Int.* 2008;17:105–112.
68. Boomi P, Ganesan R, Poorani GP, et al. Phyto-engineered gold nanoparticles (AuNPs) with potential antibacterial, antioxidant, and wound healing activities under in vitro and in vivo conditions. *Int J Nanomed.* 2020;15:7553. doi:10.2147/IJN.S257499
69. Oueslati MH, Tahar LB, Harrath AH. Catalytic, antioxidant and anticancer activities of gold nanoparticles synthesized by kaempferol glucoside from *Lotus leguminosae*. *Arab J Chem.* 2020;13(1):3112–3122. doi:10.1016/j.arabjc.2018.09.003
70. Chandrasekharan S, Chinnasamy G, Bhatnagar S. Sustainable phyto-fabrication of silver nanoparticles using *Gmelina arborea* exhibit antimicrobial and biofilm inhibition activity. *Sci Rep.* 2022;12(1):1–16. doi:10.1038/s41598-021-04025-w
71. Rajeshkumar S, Malarkodi C. In vitro antibacterial activity and mechanism of silver nanoparticles against foodborne pathogens. *Bioinorg Chem Appl.* 2014;2014:1–10. doi:10.1155/2014/581890
72. Pugazhendhi A, Kumar SS, Manikandan M, Saravanan M. Photocatalytic properties and antimicrobial efficacy of Fe doped CuO nanoparticles against the pathogenic bacteria and fungi. *Microb Pathog.* 2018;122:84–89. doi:10.1016/j.micpath.2018.06.016
73. Sondi I, Salopek-Sondi B. Silver nanoparticles as antimicrobial agent: a case study on E. coli as a model for Gram-negative bacteria. *J Colloid Interface Sci.* 2004;275(1):177–182. doi:10.1016/j.jcis.2004.02.012
74. Kota S, Dumpala P, Anantha RK, Verma MK, Kandepu S. Evaluation of therapeutic potential of the silver/silver chloride nanoparticles synthesized with the aqueous leaf extract of *Rumex acetosa*. *Sci Rep.* 2017;7(1):1–11. doi:10.1038/s41598-017-11853-2
75. Rai A, Prabhune A, Perry CC. Antibiotic mediated synthesis of gold nanoparticles with potent antimicrobial activity and their application in antimicrobial coatings. *J Mater Chem.* 2010;20(32):6789–6798. doi:10.1039/c0jm00817f

International Journal of Nanomedicine

Dovepress

Publish your work in this journal

The International Journal of Nanomedicine is an international, peer-reviewed journal focusing on the application of nanotechnology in diagnostics, therapeutics, and drug delivery systems throughout the biomedical field. This journal is indexed on PubMed Central, MedLine, CAS, SciSearch®, Current Contents®/Clinical Medicine, Journal Citation Reports/Science Edition, EMBase, Scopus and the Elsevier Bibliographic databases. The manuscript management system is completely online and includes a very quick and fair peer-review system, which is all easy to use. Visit <http://www.dovepress.com/testimonials.php> to read real quotes from published authors.

Submit your manuscript here: <https://www.dovepress.com/international-journal-of-nanomedicine-journal>